Journal of Combinatorial Mathematics
and Combinatorial Computing
www.combinatorialpress.com/jcmcc

Combinatorial Press

Network Pharmacology and Integrated Molecular Docking Study on the Mechanism of the Protective Effect of Litchi Seed in Skin Photoaging

Wenjing Yan[1], Jiajia Yin[1], Tengyu Ma[1], Yu Tian[1], Haixin Sun[1,✉]

[1] *College of Life Sciences, Qingdao University, Qingdao, Shandong, 266071, China*

ABSTRACT

Background: Ultraviolet radiation (UVR) causes premature skin aging. Litchi seed (LS) is considered a natural plant extract with potential antioxidant, anti-aging and anti-inflammatory properties. However, the mechanisms of LS's protective effects on skin photoaging remain unclear. ***Objective*:** This study aims to perform a rapid and efficient virtual screening of the main targets and possible mechanisms of the protective effect of LS on skin photoaging through network pharmacology, bioinformatics and molecular docking. ***Methods:*** The primary active compounds and their corresponding targets of LS were obtained from the TCMSP, STP, and UniProt databases. Concurrently, photoaging-related targets were mined from the GEO, GeneCards, and OMIM databases. "LS-photoaging" targets were identified using Venn diagrams created with R software. Protein-protein interaction (PPI) networks and "compound-target-disease" networks were constructed and analyzed using Cytoscape. GO and KEGG pathway enrichment analyses were then performed to predict the protective mechanisms of LS against skin photoaging. Finally, key targets and active compounds were validated through molecular docking using AutoDock Vina. ***Results:*** The screening identified 368 targets of LS active compounds and 872 photoaging-related targets. Network topology analysis revealed 87 common targets, with *AKT1*, *IL6*, *TP53*, and *CASP3* as core targets. Enrichment analysis reveals that LS can modulate the ROS/MAPK/AP-1 pathway, thereby inhibiting inflammatory responses and reducing oxidative stress, which leads to a decrease in pro-inflammatory factors. Additionally, it promotes collagen restoration by suppressing the expression of MMPs. Molecular docking validation demonstrated a strong binding affinity between the core targets and the key compounds. ***Conclusion:*** LS shows potential for treating photoaging by counteracting inflammation and oxidative stress, regulating collagen and lipid metabolism, and inhibiting apoptosis.

Keywords: bioinformatics, skin photoaging, litchi seed, network pharmacology, molecular docking, signaling pathway

✉ Corresponding author.
E-mail address: ywjqddx@126.com (H. Sun).
Received 05 March 2024; Revised 20 April 2024; Accepted 05 December 2024; Published Online 15 April 2025.
DOI: 10.61091/jcmcc127a-412

1. Introduction

The skin serves as the first important protective barrier between the body and the external environment which plays a crucial role in various physiological functions. The phenomenon of skin aging caused by ultraviolet radiation (UVR) is known as skin photoaging, which is a type of exogenous aging [1]. According to medical studies, approximately 80% of skin-related diseases are caused by exposure to UVR [2]. The damages induced by UVR in the skin elicit cellular senescence and inflammation which consequently evoke both local and systemic immunosuppression [3]. Developing plant extracts from natural products to delay skin aging not only provides a gentle and widely available solution but also addresses various skin concerns (dyspigmentation, laxity, a yellow hue, wrinkles, telangiectasia, a leathery appearance and cutaneous malignancies [4]) through multiple pathways and targets. Therefore, functional products with specialty anti-aging botanicals are also welcomed and anticipated by consumers and the market [5].

Litchi seed (LS), the dried mature seed of the soapberry family plant (*Litchi chinensis Sonn.*), is a commonly used medicinal and edible plant. With the development of modern natural products and the application of separation and analysis techniques, LS has been identified to contain various compounds such as flavonoids, steroids, phenolic acids, etc [6]. According to Chinese medicine theory, it has the effects of promoting blood circulation, dispersing stagnation, dispelling cold, and relieving pain. Modern pharmacological studies on LS have shown that it has three major effects, including antioxidant, blood glucose-lowering, and hepatoprotective effects. The active phytochemicals or the extracts of their sources have become major photoprotective strategies. Although they mainly function as antioxidants, they also display anti-inflammatory and immunomodulatory activity and also control dermal extracellular matrix remodeling [7]. LS contains a variety of polyphenols and flavonoids, including epicatechin, procyanidin A, which may be an effective compound for treating photoaging [8]. It was reported that grape seed procyanidins could be useful in the attenuation of UVR-induced oxidative stress-mediated skin diseases in human skin [9-10]. Moreover, hawthorn polyphenol extract, the main active compounds are chlorogenic acid, procyanidin B2, and epicatechin, has been shown to UVB-induced skin photoaging by regulating MMP expression and type I procollagen production in mice [11]. Another research showed that the mechanisms underlying (-)-epicatechin action may help prevent oxidative damage and modify metabolic profile [12]. Therefore, LS is very valuable for development and application in the prevention and treatment of skin photoaging effects.

Compared to traditional research on developing anti-photoaging compounds, the network pharmacology can increase the efficiency of research by rapidly screening potential drug targets or compounds through large-scale data analysis and computational methods. It is capable of integrating expertise from different fields, such as pharmacology, computer science and structural biology. In the process of analyzing the chemical compounds of drugs, organizing and modeling data on effective target points and corresponding disease target points, novel anti-photoaging compounds and pathways of action can be predicted to guide the development of drug therapy strategies [13]. Molecular docking is a theoretical simulation method based on the principles of structural biology, using computer technology to study the binding sites and affinities of target protein receptors and drug small molecule ligands [14]. Therefore, this study used network pharmacology to analyze the relevant signaling pathways and targets of the protective effect of LS on skin photoaging, and verified them through molecular docking, providing the theoretical basis for the application and development of LS extract in the prevention and treatment of skin photoaging.

2. Materials and methods

2.1. Screening of Active Compounds and Gene Targets of LS

The Traditional Chinese Medicine Systems Pharmacology Database and Analysis Platform (TCMSP: https://old.tcmsp-e.com/tcmsp.php) was used to screen the potential active compounds. According to the absorption, distribution, metabolism, and excretion (ADME) principle[15], we set the inclusion criteria as oral bioactivity (OB) $\geqslant$ 20% and drug-likeness (DL) $\geqslant$ 0.1. Active compounds that meet this criterion are considered effective. Since procyanidins are important active components of LS and have demonstrated anti-aging activity, we included procyanidin A1 and procyanidin A2 as effective active compounds as well. To ensure the accuracy of the prediction results, pharmacological targets were obtained from the TCMSP and SwissTargetPredict (STP: http://www.swisstargetprediction.ch/index.php) databases. The target protein names were then converted into official gene symbols using the Universal Protein Resource (UniProt: http://www.uniprot.org) database [16].

2.2. Gathering of Skin Photoaging-related Targets

Skin photoaging-related targets were gathered using the Gene Expression Omnibus (GEO) database (GEO: https://www.ncbi.nlm.nih.gov/geo/), with "Skin Photoaging" as the search term and "Homo sapiens" as the species restriction. The GEO database enabled differential analysis of microarrays, which can be used to screen for networks of genes that are differentially expressed in specific environments, such as diseases [17]. Based on the sample size and the quality of the microarray, the GSE192564 datasets and the GSE192565 datasets were selected for differential expression analysis of skin photoaging genes. Photoaging freckle disease was a photoaging lesion caused by long-term exposure of the skin to sunlight, and was considered to be one of the clinical manifestations of skin photoaging. The GSE192564 datasets and GSE192565 datasets consist of the photodamage freckle disease group and the non-lesion control group [18]. Differentially expressed genes (DEGs) analysis was realized by R version 4.2.0, which successively uses the GEO query package [19] to complete the data download and the limma package [20] to complete the differential analysis. The screening conditions were set as $P<0.05$, $|logFC|>0.5$ (FC denotes the number of times of difference). The analysis results were used to complete data visualization using the ggplot2 package [21].

"Skin Photoaging" were used as the keywords to obtain targets from Online Mendelian Inheritance in Man (OMIM: https://omim.org/) and Genecards (Genecards: https://www.genecards.org/), "*Homo sapiens*" was set as the species type to get the target name and remove duplicates. Finally, DEGs from GEO database, highly correlated gene targets from Genecards database, and gene targets from OMIM database were merged to get skin photoaging related gene targets.

2.3. The Common Targets Overlapped between Active Compounds and Photoaging-related Targets

The targets of LS obtained from 2.1 and the targets of skin photoaging gathered from 2.2 were merged and intersected. R version 4.2.0 was used to draw a Venn plot, where LS gene targets and skin photoaging gene targets were imported to identify their intersection. The intersecting parts of the Venn plot were outputted as common targets.

2.4. Construction of Protein-protein Interaction Network

The common targets between LS and skin photoaging were imported into the STRING database (STRING: https://string-db.org/), a tool for finding interacting genes and proteins. The species was limited to "*Homo sapiens*", and a confidence score threshold of > 0.7 was applied to construct the protein-protein interaction (PPI) network. Then, visual network analysis was plotted by Cytoscape version 3.9.1. The core targets above the median values of degree centrality (DC), betweenness

centrality (BC) and closeness centrality (CC) were obtained from the CytoNCA analysis[22]. The hub targets of LS in treating skin photoaging were screened by Cytohubba, an analysis tool of Cytoscape 3.9.1.

2.5. GO and KEGG Enrichment Analyses

The Gene Ontology (GO) functional enrichment, Kyoto Encyclopedia of Genes and Genomes (KEGG) pathway enrichment analyses and signaling pathway enrichment analysis of the common "LS-Photoaging" targets were performed using the R packages ("clusterProfiler", "org.Hs.eg.db", "enrichplot", "ggplot2" and "pathview"). Enrichment analysis using R version 4.2.0. with $P < 0.05$ as conditions.

2.6. "Compound-target-disease" Network Establishment

Cytoscape version 3.9.1 was used to construct the "compound-target-disease" topology network, to clarify the connection between the LS's active compounds and "Drug-Disease" targets scientifically. Using the CytoNCA plug-in for topological analysis and visualization of network parameters, node color and size were determined according to the degree value [23].

2.7. Molecular Docking

Selection of active components with meaningful topological network as ligands for docking with core protein receptors. The protein receptor IDs were determined by referring to the UniProt database. Subsequently, the corresponding core target protein receptor structures were retrieved and downloaded from the RCSB Protein Data Bank using the IDs obtained from UniProt in RCSB Protein Data Bank (RCSB PDB: https://www.rcsb.org/). The receptor structures were preprocessed using PyMOL version 3.0.0 (PyMOL: https://www.pymol.org/) by removing water molecules and irrelevant residues. The structures of active compound compounds were obtained from PubChem database (PubChem: https://pubchem.ncbi.nlm.nih.gov/) [24]. After determining the receptor and ligand structures, the AutoDock Tools version 1.5.7 (ADT: https://autodock.scripps.edu/) was used for grid box parameter setup, and spatial parameters were obtained. Subsequently, the AutoDock Vina (https://vina.scripps.edu) was employed for docking to obtain binding affinity values. The ligand-receptor combinations with good binding affinity were visualized using PyMOL [25]. Docking results for AutoDock Vina were presented as heatmaps using the Graphpad Prism version 9.5 (https://www.graphpad-prism.cn/).

3. Results

3.1. LS Active Compounds and Targets

The inclusion criteria were set as oral bioactivity (OB) $\geqslant$ 20% and drug likeness (DL) $\geqslant$ 0.1. Based on these criteria, the TCMSP database was utilized to screen and obtain 23 active compounds from LS. The effective active compounds of LS were shown below (Table 1). A total of 368 pharmacological targets were obtained through a search of the TCMSP and STP databases.

Table 1. LS active compounds

MOL ID	Name	MW(g/mol)	OB ⩾ 20%	DL ⩾ 0.1
MOL010690	Butyl oleate	338.64	30.13	0.25
MOL010691	Ethyl palmitelaidate	282.52	34.93	0.14
MOL000131	Linoleic Acid	280.50	41.90	0.14
MOL001494	Mandenol	308.56	42.00	0.19
MOL001600	Copaene	204.39	29.47	0.12
MOL001641	Methyl linoleate	294.53	41.93	0.17
MOL000256	Glyceryl Trioleate	885.61	27.27	0.13
MOL002573	β-patchoulene	204.39	50.69	0.11
MOL002883	Ethyl oleate	310.58	32.40	0.19
MOL003538	Viridiflorene	204.39	51.84	0.10
MOL000357	Sitogluside	576.95	20.63	0.62
MOL000358	Beta-Sitosterol	414.79	36.91	0.75
MOL000359	Sitosterol	414.79	36.91	0.75
MOL000449	Stigmasterol	412.77	43.83	0.76
MOL002003	(-)-Caryophyllene oxide	220.39	32.67	0.13
MOL000057	Diisobutyl phthalate	278.38	49.63	0.13
MOL000066	alloaromadendrene	204.39	53.46	0.10
MOL000675	Oleic Acid	282.52	33.13	0.14
MOL000676	Dibutyl Phthalate	278.38	64.54	0.13
MOL000073	ent-Epicatechin	290.29	48.96	0.24
MOL000098	Quercetin	302.25	46.43	0.28
MOL010491	Procyanidin A1	576.54	15.07	0.40
MOL007294	procyanidin A2	576.54	12.25	0.40

Note: MW: molecular weight, refers to the mass of a molecule. DL: drug-likeness, DL is a qualitative concept used in drug design for an estimate on how "drug-like" a prospective compound is, which helps to optimize pharmacokinetic and pharmaceutical properties, such as solubility and chemical stability[26]. OB: Oral bioavailability, OB represents the percentage of an orally administered dose of unchanged drug that reaches the systemic circulation, which reveals the convergence of the ADME process. High oral bioavailability is often a key indicator to determine the drug-like property of bioactive molecules as therapeutic agents.

3.2. Acquisition of Skin Photoaging Gene Targets

After conducting differential analysis on the GSE192564 datasets and GSE192565 datasets, a total of 374 up-regulated genes and 328 down-regulated genes were identified. The analysis results were visualized in the form of the gene heat maps (Figure 1**A** and 1**B**) and volcano plots (Figure 1**C** and 1**D**). Heatmaps cluster the existing groups in the dataset, while volcano plots show the up-regulation and down-regulation relationships of genes, with red indicating up-regulation and blue indicating down-regulation. The GeneCards database and OMIM database did not require data analysis, and the screening process could be completed by importing the screening results into an Excel sheet. The results were merged, and duplicates were removed as part of the analysis. After sorting, we obtained 130 and 284 targets from OMIM database and Genecards database, respectively. The 474 differentially expressed genes (DEGs) were obtained based on the analysis of the GSE192564 datasets and GSE192565 datasets in the GEO database. After integration, a total of 872 pathological target genes were acquired.

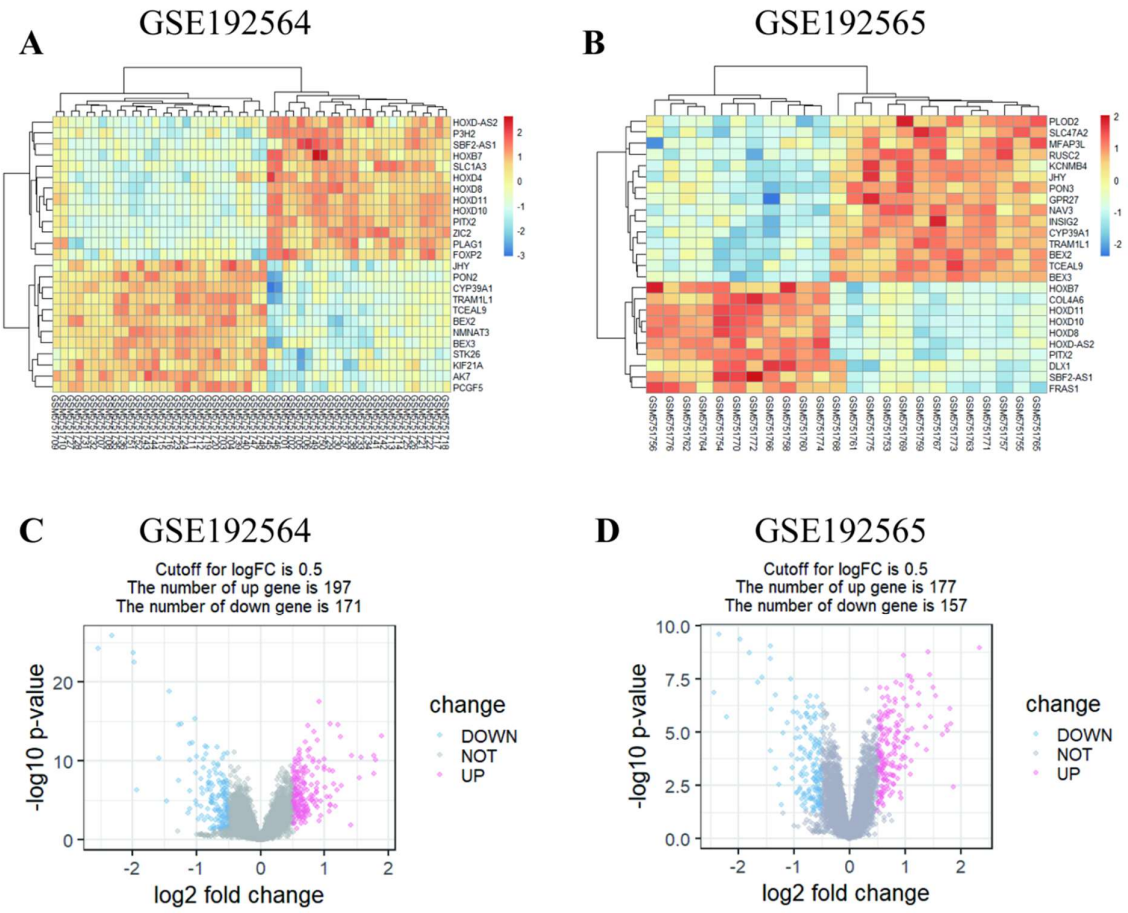

Fig. 1. The GEO differential gene analysis results. (A) Heatmap of GSE192564 differential genes. (B) Heatmap of GSE192565 differential genes. (C) Volcano plot of GSE192564 differential genes. (D) Volcano plot of GSE192565 differential genes.

3.3. Intersecting Gene Targets

The LS targets screened in 3.1. and the skin photoaging targets obtained in 3.2. were taken to be intersected by Venn diagram to obtain 87 intersecting gene targets (Figure2, Table 2). These 87 common targets are considered to be promising targets for the treatment of photoaging with LS.

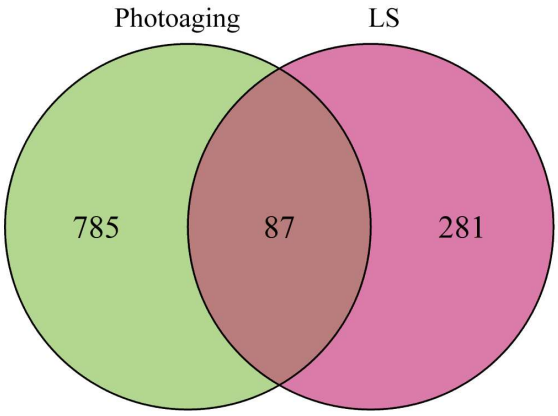

Fig. 2. Intersection of LS targets and photoaging targets

Table 2. The 87 common targets between active compound targets of LS and photoaging disease.

No.	Target	No.	Target	No.	Target	No.	Target	No.	Target	No.	Target
1	TP53	16	VEGFA	31	MMP13	46	CTSD	61	GLO1	76	CA13
2	CDKN2A	17	MMP9	32	CASP8	47	ESR2	62	HSF1	77	IGFBP3
3	PTEN	18	EGF	33	PPARA	48	XDH	63	TEP1	78	AR
4	COL1A1	19	MAPK1	34	TRPV1	49	MMP12	64	EGFR	79	LYZ
5	AKT1	20	JUN	35	SOD1	50	CTSL	65	TYR	80	PLAU
6	IL6	21	PPARG	36	NFKBIA	51	BCL2L1	66	PTGER3	81	ADRB1
7	MMP1	22	FOS	37	NOS2	52	SULT1E1	67	PTGS1	82	VCAM1
8	MYC	23	CDKN1A	38	BAX	53	ALOX5	68	HTR3A	83	HSD17B2
9	COL3A1	24	CHUK	39	MIF	54	CASP9	69	PYGL	84	DPP4
10	IL1B	25	ESR1	40	CYP1B1	55	CHRNA7	70	ODC1	85	ABCG2
11	PIK3R1	26	NFE2L2	41	SCD	56	PTK2	71	CCL2	86	SELE
12	TGFB1	27	CAT	42	PRKCD	57	HAS2	72	CHRM3	87	PTGS2
13	CTSB	28	CASP3	43	PPARD	58	NR1H3	73	BCHE		
14	MMP2	29	MMP3	44	PIK3CG	59	ACACA	74	HSD11B1		
15	IL1A	30	HIF1A	45	RXRA	60	NOX4	75	ALOX12		

3.4. Analysis and Construction of PPI Network

The PPI network of anti-photoaging targets of LS was constructed using the STRING database and visualized with Cytoscape 3.9.1 software, as depicted in Figure 3**A**. In this network, the size and color of the nodes represent the target degree value. Degree centrality (DC) was employed as a plotting metric due to its intuitive representation of node centrality[27]. Utilizing the CytoHubba plugin, the top 10 hub genes were identified based on the MCC method (Figure 3**B**). A core PPI network was delineated through topology analysis, using a threshold of $\geqslant$ 2 times the median DC, with the median DC, CC, and BC values being 16, 0.65, and 7.7, respectively. This analysis revealed 17 core targets (Figure 3**C**). Consequently, the core targets of LS against skin photoaging were determined to be AKT1, IL6, TP53, CASP3, JUN, and IL1B.

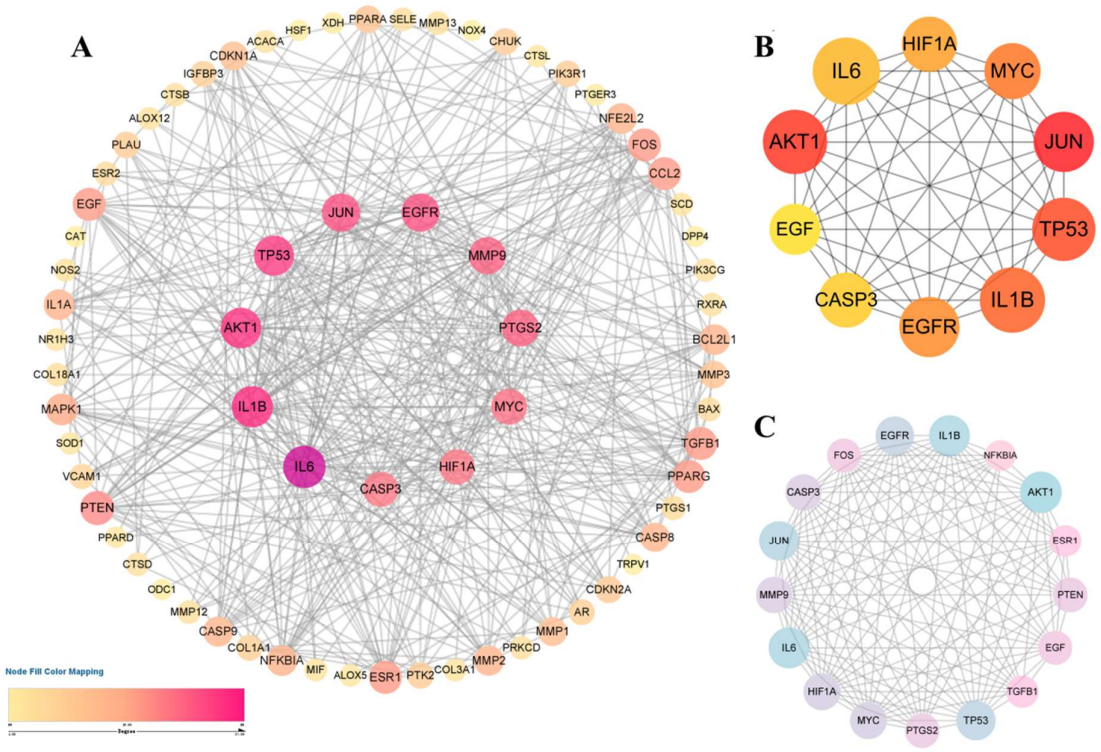

Fig. 3. The protein-protein interaction (PPI) analysis results. (A) Identification of candidate targets via PPI analysis and the topological screening for the PPI network. Shown in the lower left corner were correspondence of node size and color to target degree value. (B) The hub genes were selected from the PPI network using the CytoHubba plugin. The node color was from pale yellow to red, and the corresponding degree gradually larger. (C) 17 core genes obtained after topological screening of DC, BC, and CC for intersecting targets.

3.5. GO and KEGG Enrichment Analysis

The GO enrichment analysis and KEGG pathway enrichment analysis of "LS-Photoaging" targets using R software at a screening threshold $P < 0.05$. The GO functional enrichment results elucidated the role of intersecting genes in three ways. The top 10 for each entry are shown in bar and bubble charts (Figure 4**A** and 4**C**). The inter-correspondence between GO terms and targets involved in enrichment is shown in a cnet diagram (Figure 4**E**). The Biological Processes (BP) terms were mainly enriched in response to reactive oxygen species, response to oxidative stress, epithelial cell proliferation and response to UV. The Molecular function (MF) terms mainly included DNA–binding transcription factor binding, RNA polymerase II–specific DNA–binding transcription factor binding, endopeptidase activity and cytokine receptor binding. In addition, the highly enriched cellular components (CC) terms were vesicle lumen,secretory granule lumen and cytoplasmic vesicle lumen.

The KEGG pathway enrichment analysis showed that the major pathways associated with the target genes involve chemical carcinogenesis – reactive oxygen species, the TNF signaling pathway, the IL–17 signaling pathway, apoptosis, multiple cancer-related pathways and multiple inflammatory and infection signaling pathways. The top 20 pathways are plotted as bar charts and bubble charts according to the degree of enrichment (Figure 4**B** and 4**D**). Additionally, a cnet diagram (Figure 4F) was constructed using R software to illustrate the connections between the target genes and the enriched pathways.

The high enrichment for the reactive oxygen species (ROS) activation pathway and the IL-17 signaling pathway indicated that LS may act through these two pathways in the treatment of

photoaging. We visualized the two KEGG pathways using "pathview" in R (Figure 5**A and** 5**B**). Among others, stimulated by UVR, epidermal growth factor (EGF) binds to the epidermal growth factor receptor (EGFR) and subsequently activates the ROS/MAPK/AP-1signaling pathways. In the MAPK pathway, MAPK is responsible for the activation of downstream activating protein 1 (AP-1), which subsequently upregulates the expression of the matrix metalloproteinase (MMP) family, thereby triggering an inflammatory response. Our pathway visualization suggests that LS mitigates photoaging primarily by inhibiting this signaling cascade.

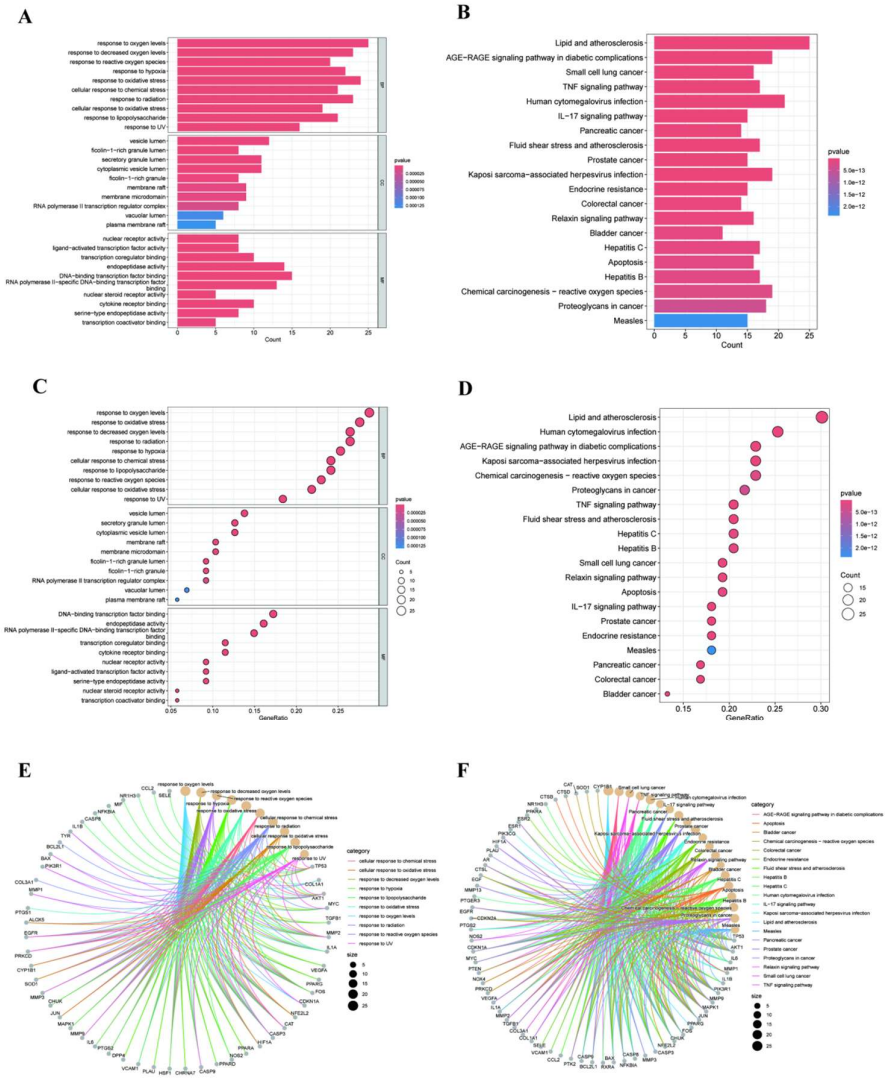

Fig. 4. Visualization of GO enrichment analysis and KEGG pathway enrichment results. (A) The bar diagram of GO enrichment analysis results. (B)The bar diagram of KEGG pathway enrichment analysis results (C) The bubble diagram of GO enrichment analysis results. (D) The bubble diagram of GO enrichment analysis results. (E) The targets-to-terms correspondence cnet diagram for GO enrichment analysis. (F) The cnet diagram of the KEGG pathway analysis of the therapeutic targets of LS in photoaging treatment. The left round nodes of the cnet diagram represent the therapeutic targets, the right round nodes of the cnet diagram represent the KEGG pathways, and the lines represent the ownership of targets and pathway.

A

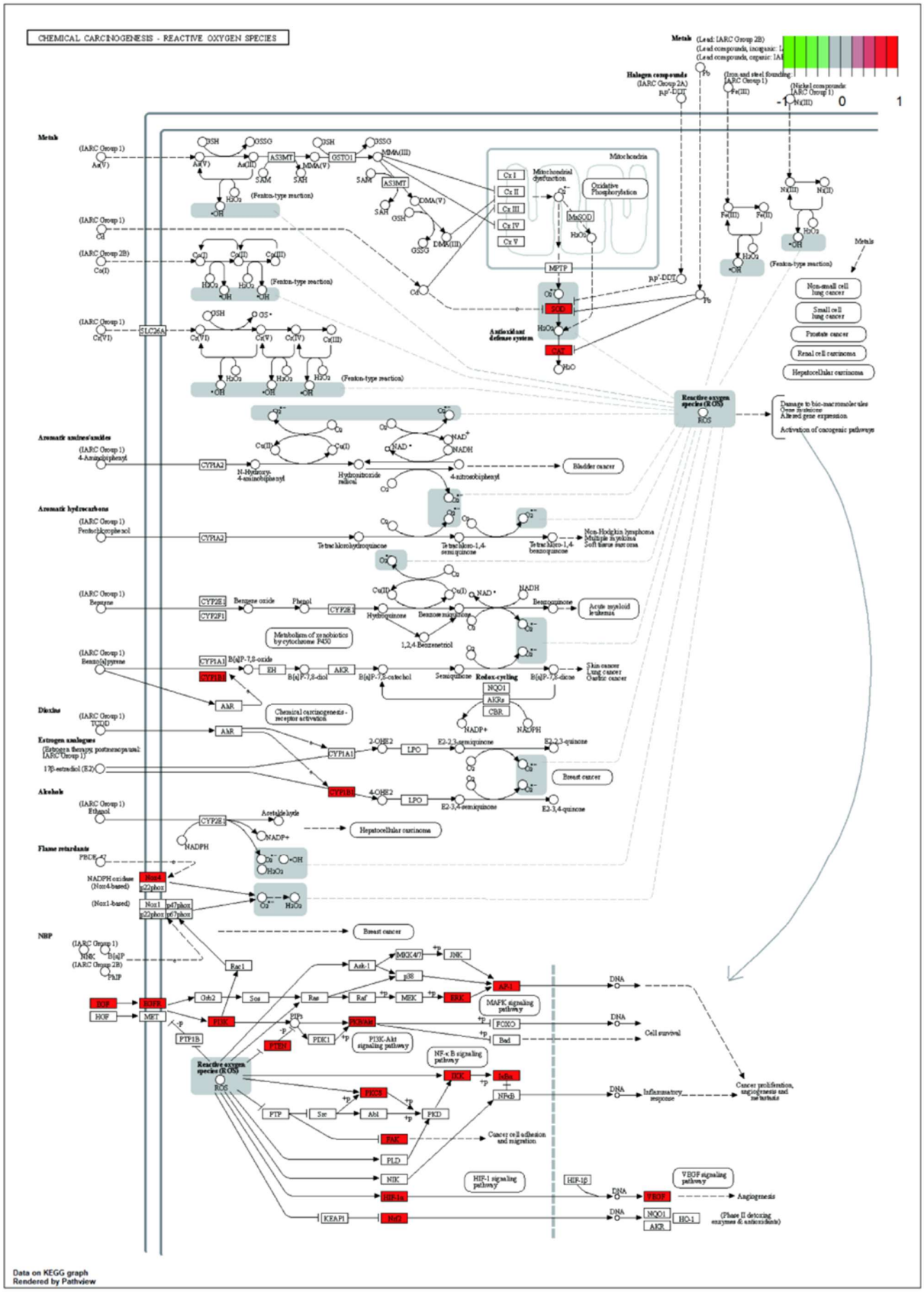
CHEMICAL CARCINOGENESIS - REACTIVE OXYGEN SPECIES
Metals
Halogen compounds
Mitochondria
Oxidative Phosphorylation
Antioxidant defense system
Reactive oxygen species (ROS)
Non-small cell lung cancer
Small cell lung cancer
Prostate cancer
Renal cell carcinoma
Hepatocellular carcinoma
Aromatic amines/amides
Bladder cancer
Aromatic hydrocarbons
Acute myeloid leukemia
Dioxins
Estrogen analogues
Breast cancer
Alcohols
Flame retardants
NBP
MAPK signaling pathway
PI3K-Akt signaling pathway
NF-κB signaling pathway
HIF-1 signaling pathway
VEGF signaling pathway
Cell survival
Cancer cell adhesion and migration
Angiogenesis
Data on KEGG graph
Rendered by Pathview

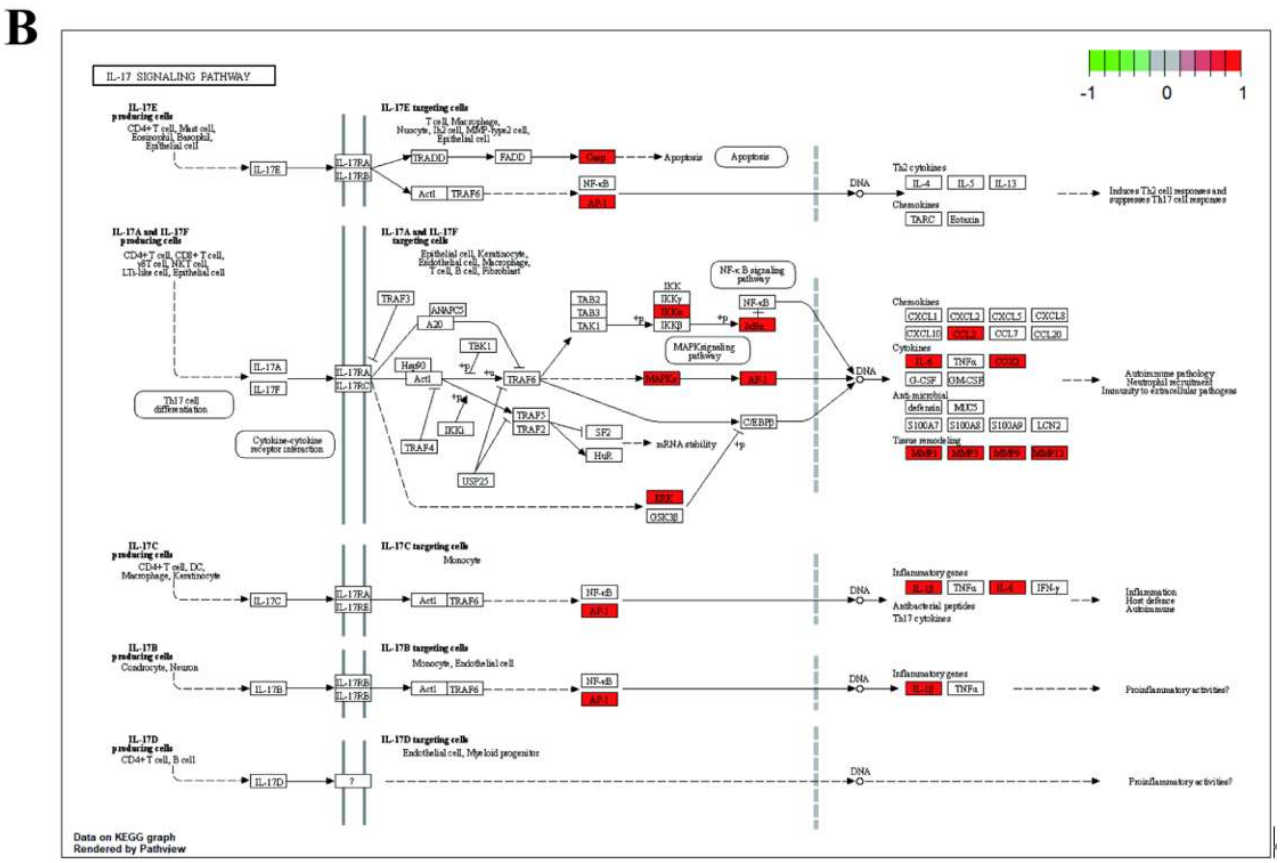

Fig. 5. Distribution of key targets in the most related pathways. (A) Distribution of key targets in the IL-17 signaling pathway. (B) Distribution of key targets in the reactive oxygen species activation pathway. The red rectangle stands for the key targets. The putative targets and the genes implicated in the pathway are shown in red.

3.6. "Compound-target-disease" Network Diagram Construction and Analysis

The "compound-target-disease" network diagram was constructed using Cytoscape (Figure 6). In the network diagram, the blue nodes were all the intersecting targets of LS action on photoaging. The green nodes showed the contribution of all active compounds in the drug to the "LS-photoaging" target, with the node size proportional to the degree value. From the network diagram analysis, quercetin, ent-Epicatechin, stigmasterol, β-sitosterol, and procyanidin A1 among the active ingredients of LS were the core compounds for the treatment of photoaging. Additionally, the network diagram of effective compounds-targets-pathways also demonstrated that LS exerts its protective effects against skin photoaging through multiple compounds and targets.

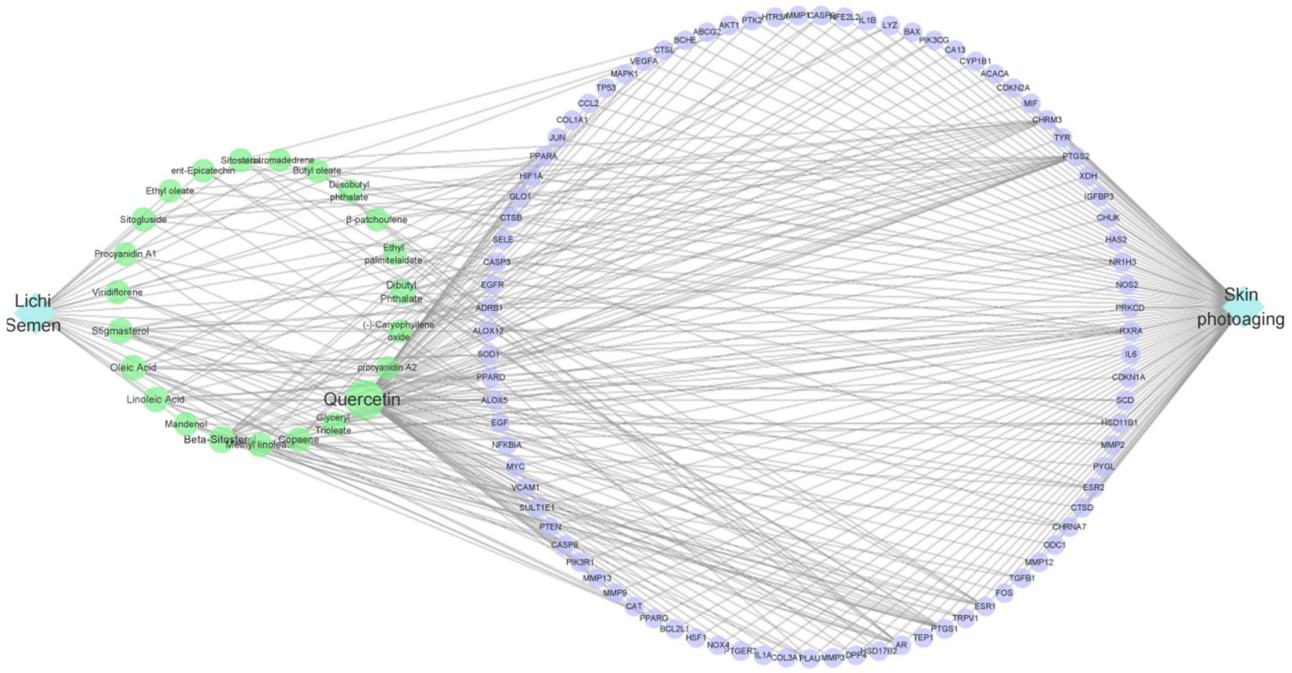

Fig. 6. "Compounds-targets-disease" interaction network diagram.The diamond-shaped targets represent drugs and diseases, respectively. The green circular targets represent active compounds, and the purple circular targets represent genes.

3.7. Molecular Docking Verification of Key Compounds and Key Targets

Through the analysis of the "compounds-targets-disease" interaction network diagram (Figure 6) and the investigation of the effective potential components against photoaging, a total of 5 core compounds are identified, namely quercetin, β-sitosterol, procyanidin A1, stigmasterol, and ent-epicatechin. By screening the PPI network (Figure3**B** and 3**C**) and analysing the target-pathway cnet diagram (Figure4**F**), a total of 4 core targets are identified, namely AKT1, IL6, TP53 and CASP3. The core compounds are then subjected to molecular docking validation with the core targets to evaluate their binding interactions and affinities with the respective receptors (Figure7 and Figure8). The binding energy results, displayed in the heatmap, indicate strong binding affinities between target proteins and compounds when the binding energy is significantly lower than -7 kcal/mol. After docking 20 receptor-ligand molecular pairs, it was found that 15 pairs exhibited binding energies less than -7 kcal/mol. The interactions and binding modes of the compounds and targets, characterized by high free binding energy scores, were visualized using PyMOL.

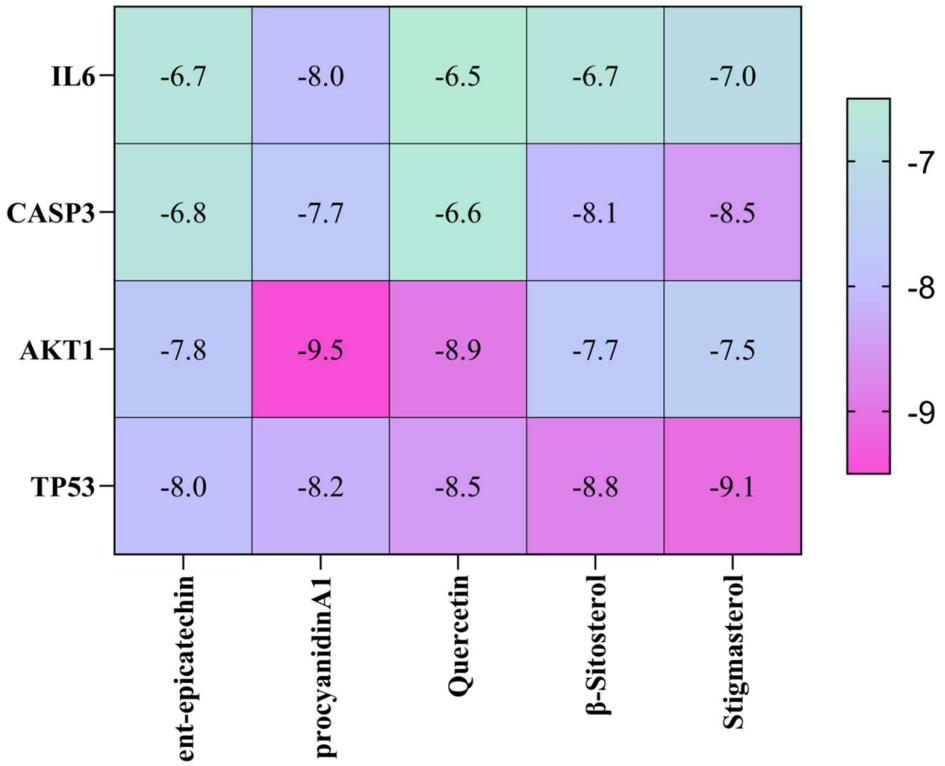

Fig. 7. Heatmap of molecular docking scores and visualization of some docking results of key compounds of LS and key targets of photoaging (The number marked in the heat map square is the docking score, the darker the square the lower the docking score, the better the docking effect.)

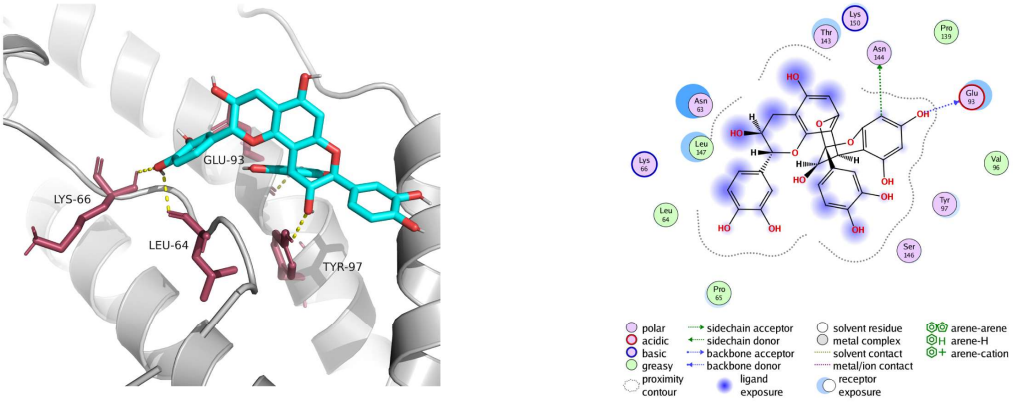
GLU-93
LYS-66
LEU-64
TYR-97
polar
acidic
basic
greasy
proximity contour
sidechain acceptor
sidechain donor
backbone acceptor
backbone donor
ligand exposure
solvent residue
metal complex
solvent contact
metal/ion contact
receptor exposure
arene-arene
arene-H
arene-cation

(A)

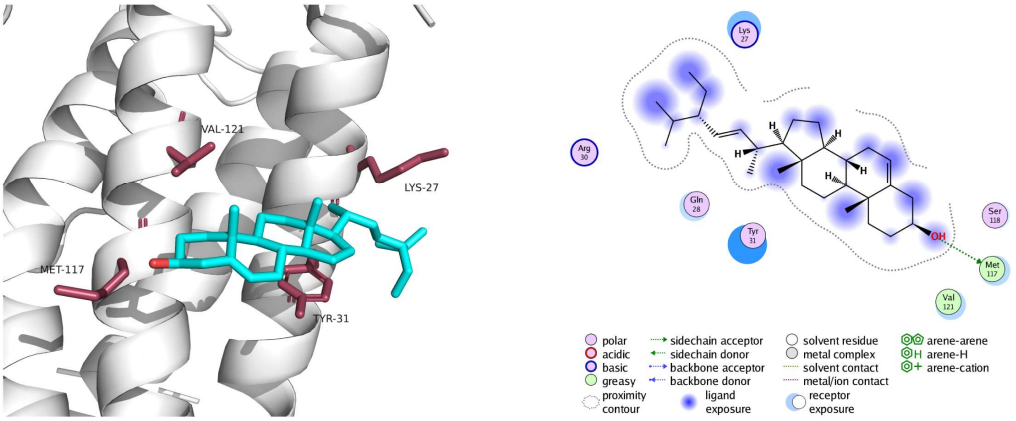
VAL-121
LYS-27
MET-117
TYR-31
polar
acidic
basic
greasy
proximity contour
sidechain acceptor
sidechain donor
backbone acceptor
backbone donor
ligand exposure
solvent residue
metal complex
solvent contact
metal/ion contact
receptor exposure
arene-arene
arene-H
arene-cation

(B)

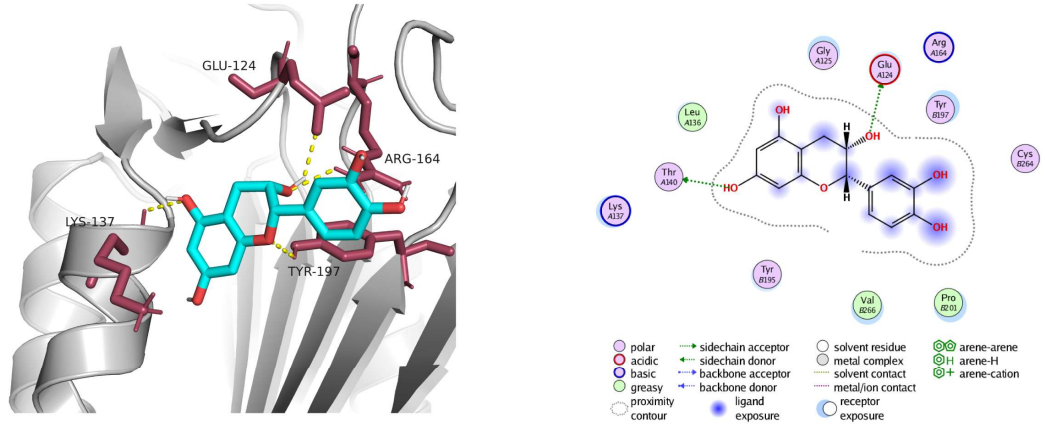
GLU-124
ARG-164
LYS-137
TYR-197
polar
acidic
basic
greasy
proximity contour
sidechain acceptor
sidechain donor
backbone acceptor
backbone donor
ligand exposure
solvent residue
metal complex
solvent contact
metal/ion contact
receptor exposure
arene-arene
arene-H
arene-cation

(C)

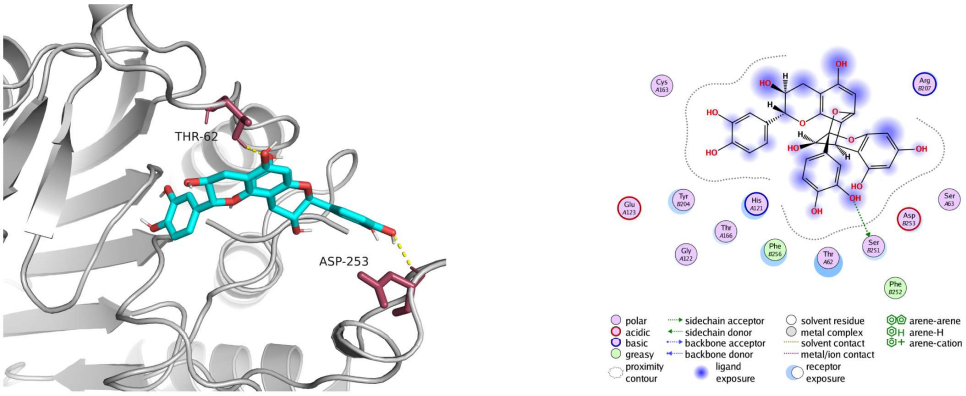
THR-62
ASP-253
polar
acidic
basic
greasy
proximity contour
sidechain acceptor
sidechain donor
backbone acceptor
backbone donor
ligand exposure
solvent residue
metal complex
solvent contact
metal/ion contact
receptor exposure
arene-arene
arene-H
arene-cation

(D)

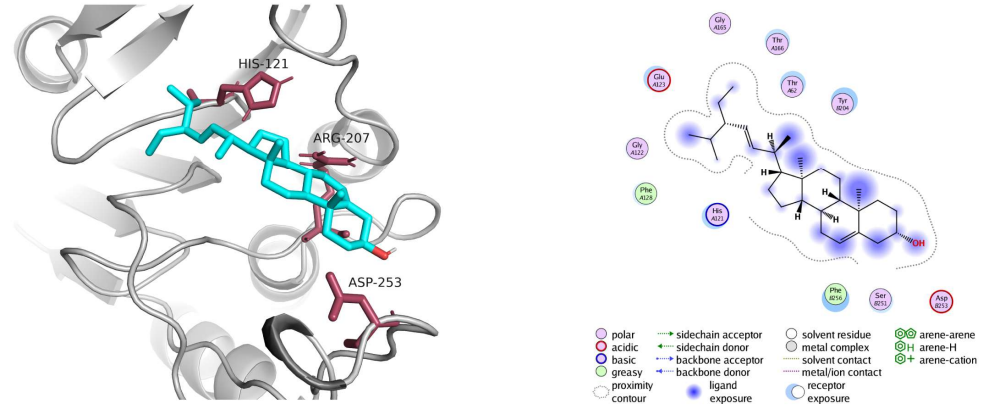
HIS-121
ARG-207
ASP-253
polar
acidic
basic
greasy
proximity contour
sidechain acceptor
sidechain donor
backbone acceptor
backbone donor
ligand exposure
solvent residue
metal complex
solvent contact
metal/ion contact
receptor exposure
arene-arene
arene-H
arene-cation

(E)

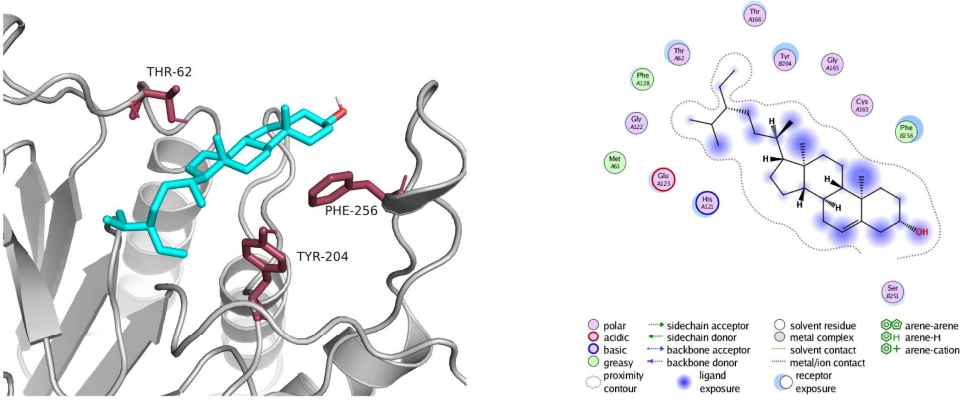
THR-62
PHE-256
TYR-204
polar
acidic
basic
greasy
proximity contour
sidechain acceptor
sidechain donor
backbone acceptor
backbone donor
ligand exposure
solvent residue
metal complex
solvent contact
metal/ion contact
receptor exposure
arene-arene
arene-H
arene-cation

(F)

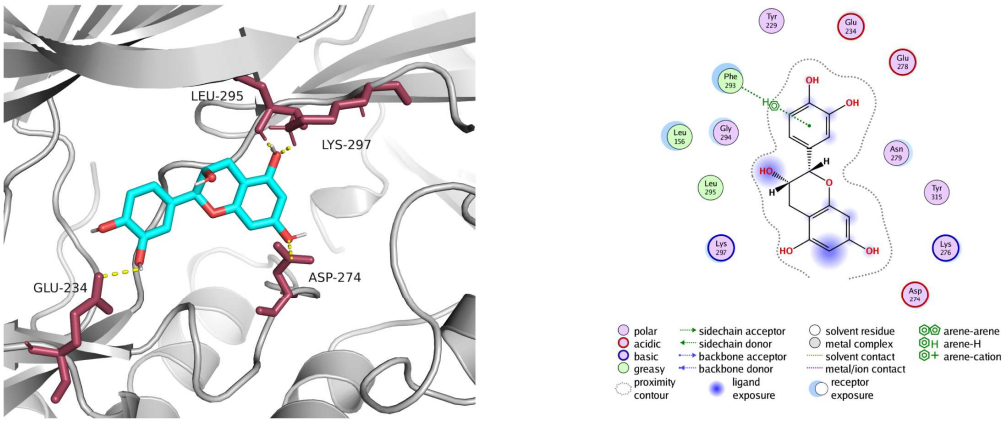
LEU-295
LYS-297
GLU-234
ASP-274
polar
acidic
basic
greasy
proximity
contour
sidechain acceptor
sidechain donor
backbone acceptor
backbone donor
ligand
exposure
solvent residue
metal complex
solvent contact
metal/ion contact
receptor
exposure
arene-arene
arene-H
arene-cation

(G)

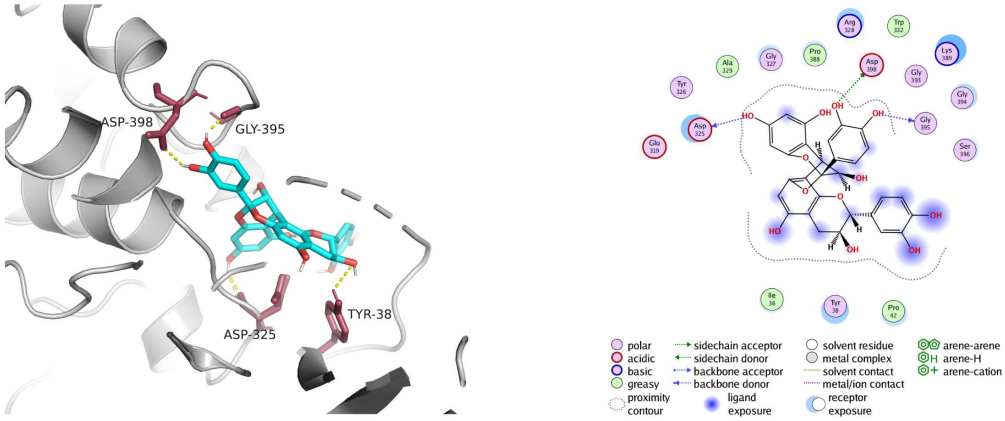
ASP-398
GLY-395
TYR-38
ASP-325
polar
acidic
basic
greasy
proximity
contour
sidechain acceptor
sidechain donor
backbone acceptor
backbone donor
ligand
exposure
solvent residue
metal complex
solvent contact
metal/ion contact
receptor
exposure
arene-arene
arene-H
arene-cation

(H)

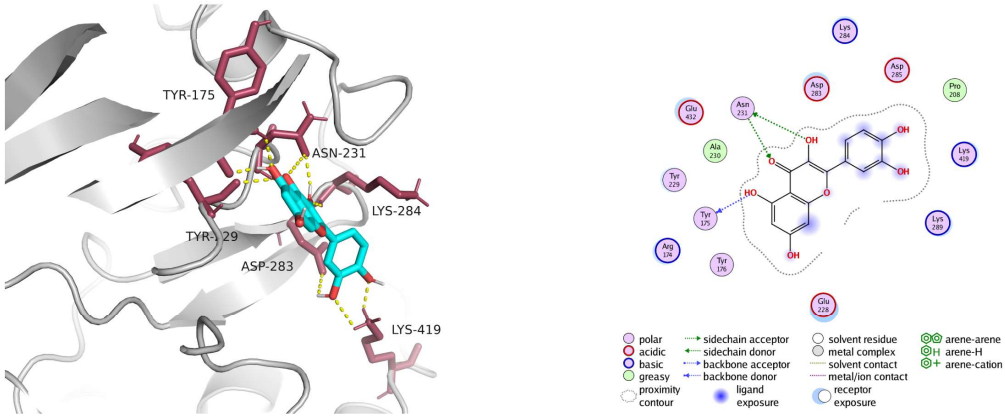
TYR-175
ASN-231
LYS-284
TYR-29
ASP-283
LYS-419
polar
acidic
basic
greasy
proximity
contour
sidechain acceptor
sidechain donor
backbone acceptor
backbone donor
ligand
exposure
solvent residue
metal complex
solvent contact
metal/ion contact
receptor
exposure
arene-arene
arene-H
arene-cation

(I)

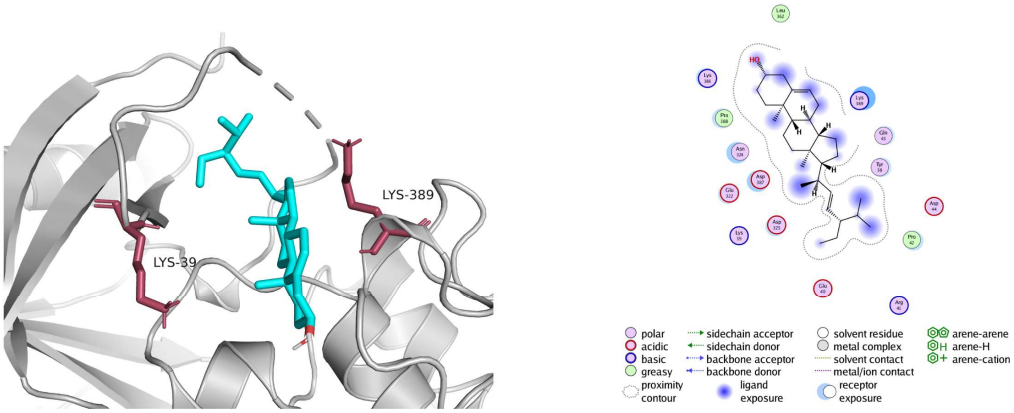
LYS-389
LYS-39
polar
acidic
basic
greasy
proximity
contour
sidechain acceptor
sidechain donor
backbone acceptor
backbone donor
ligand
exposure
solvent residue
metal complex
solvent contact
metal/ion contact
receptor
exposure
arene-arene
arene-H
arene-cation

(J)

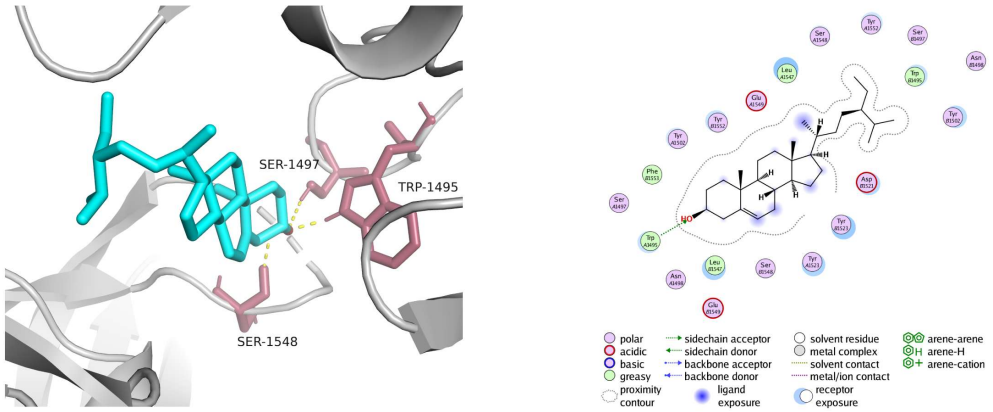
SER-1497
TRP-1495
SER-1548
polar
acidic
basic
greasy
proximity
contour
sidechain acceptor
sidechain donor
backbone acceptor
backbone donor
ligand
exposure
solvent residue
metal complex
solvent contact
metal/ion contact
receptor
exposure
arene-arene
arene-H
arene-cation

(K)

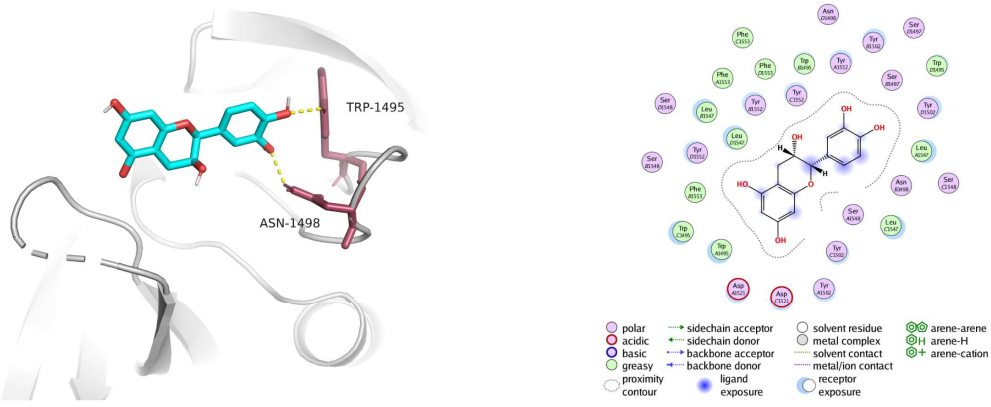
TRP-1495
ASN-1498
polar
acidic
basic
greasy
proximity
contour
sidechain acceptor
sidechain donor
backbone acceptor
backbone donor
ligand
exposure
solvent residue
metal complex
solvent contact
metal/ion contact
receptor
exposure
arene-arene
arene-H
arene-cation

(L)

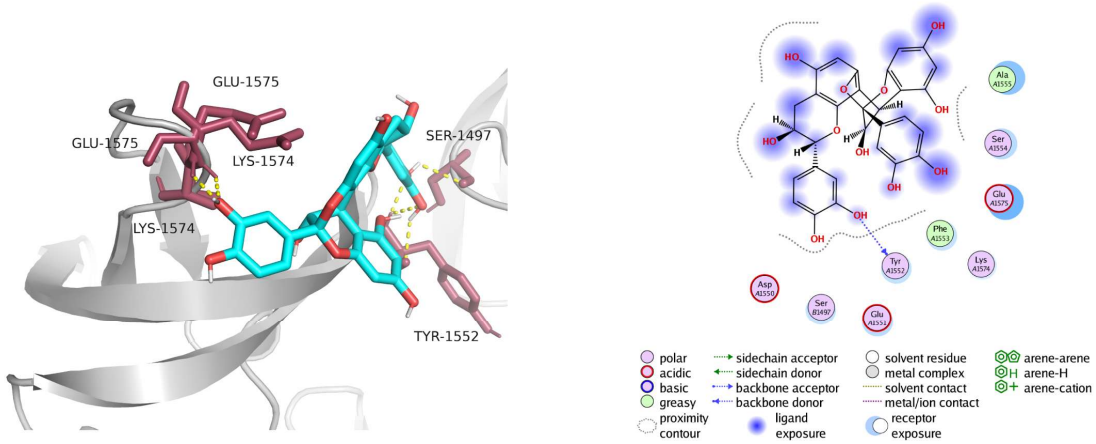
GLU-1575
GLU-1575
LYS-1574
SER-1497
LYS-1574
TYR-1552
polar
acidic
basic
greasy
proximity contour
sidechain acceptor
sidechain donor
backbone acceptor
backbone donor
ligand exposure
solvent residue
metal complex
solvent contact
metal/ion contact
receptor exposure
arene-arene
arene-H
arene-cation

(M)

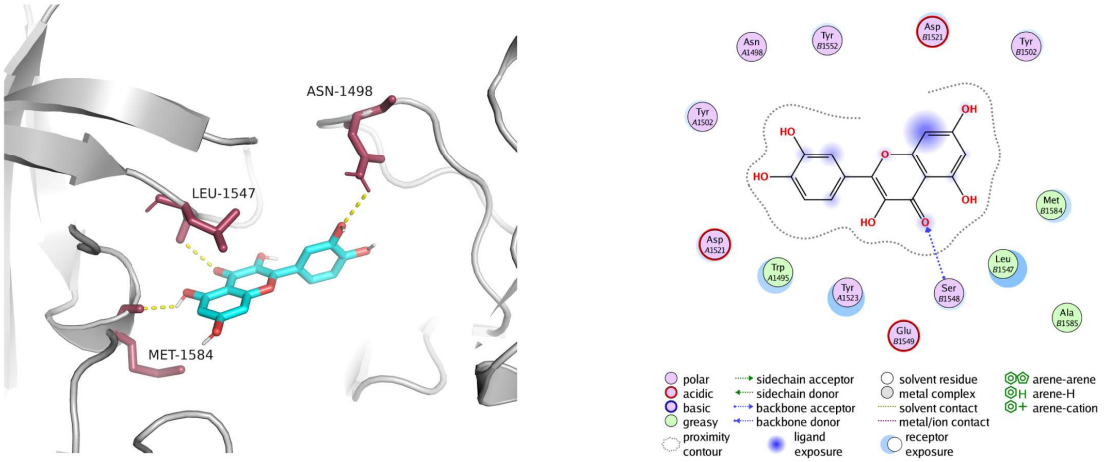
ASN-1498
LEU-1547
MET-1584
polar
acidic
basic
greasy
proximity contour
sidechain acceptor
sidechain donor
backbone acceptor
backbone donor
ligand exposure
solvent residue
metal complex
solvent contact
metal/ion contact
receptor exposure
arene-arene
arene-H
arene-cation

(N)

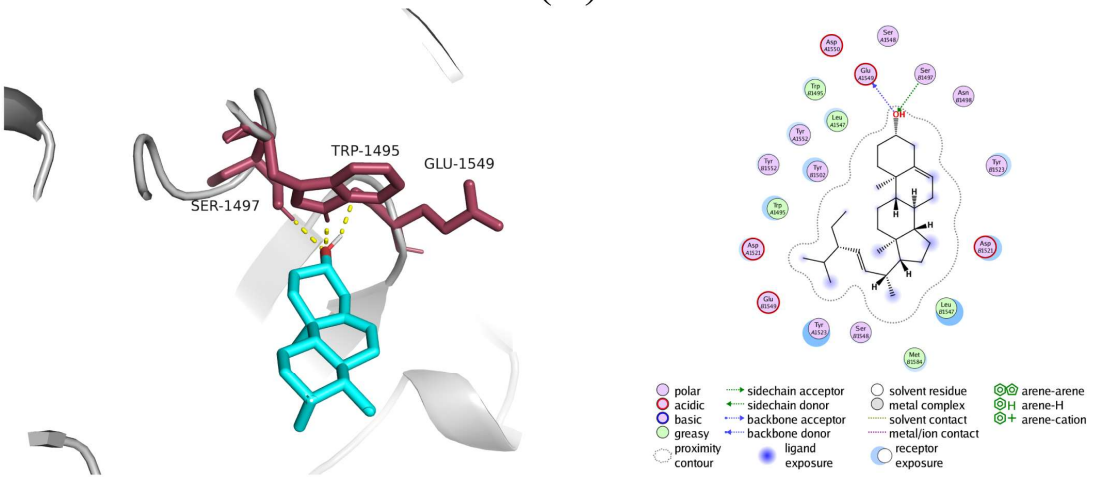
TRP-1495
GLU-1549
SER-1497
polar
acidic
basic
greasy
proximity contour
sidechain acceptor
sidechain donor
backbone acceptor
backbone donor
ligand exposure
solvent residue
metal complex
solvent contact
metal/ion contact
receptor exposure
arene-arene
arene-H
arene-cation

(O)

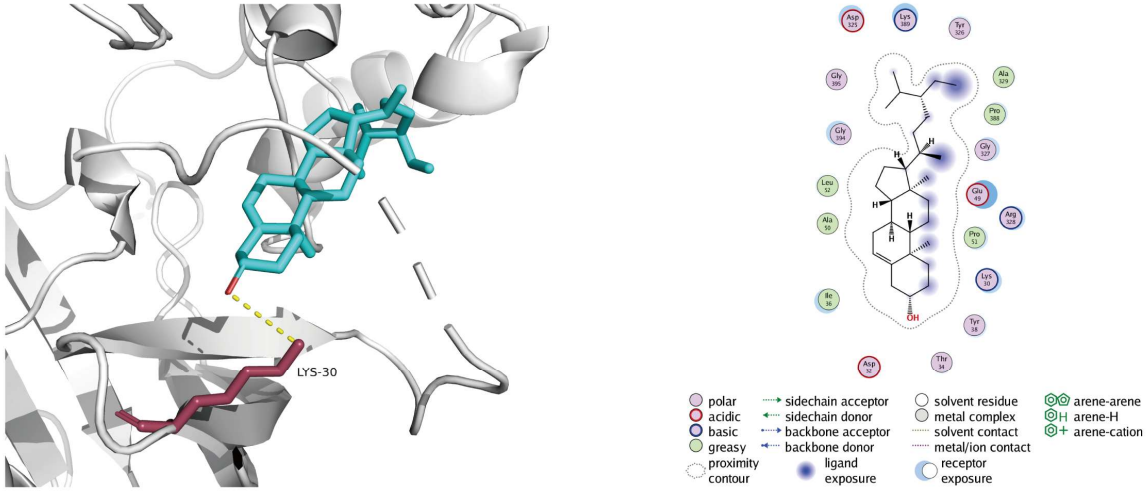

(P)

Fig. 8. Molecular docking results. (A) IL6 (PDB ID: 1ALU) with ent-epicatechin. (B) IL6 with procyanidin A1. (C) CASP3 (PDB ID: 2DKO) with ent-epicatechin. (D) CASP3 with procyanidin A1. (E) CASP3 with stigmasterol. (F) CASP3 with β-sitosterol. (G) AKT1(PDB ID:7NH5) with ent-epicatechin. (H) AKT1 with procyanidin A1. (I) AKT1 with quercetin. (J) AKT1 with stigmasterol. (K) TP53 (PDB ID: 8EOM) with β-sitosterol. (L) TP53 with ent-epicatechin. (M) TP53 with procyanidin A1. (N) TP53 with quercetin. (O) TP53 with stigmasterol. (P) AKT1(PDB ID:7NH5) with β-sitosterol.

4. Discussion

Skin aging is a complex biological process. Endogenous aging is controlled by genetic factors and progresses with age. In contrast, exogenous aging is triggered by external environmental stressors, with photoaging caused by ultraviolet radiation (UVR) being a significant contributor. Photoaging is mainly manifested by causing skin damage, skin malignant tumors, premature aging, and overproduction of melanin[28]. In the dermis, UVR induces the production of ROS, and elevated ROS can cause a series of oxidative stress reactions. The active ingredients in natural plant extracts are important antioxidants[29]. In order to enhance the intrinsic antioxidant defense mechanism and restore the normal physiological state of the skin, the introduction of antioxidants through dietary means or through topical application as cosmetic formulations has become an important means of solving all types of skin-related diseases[30]. Lychee seed (LS) has long been utilized in traditional Chinese medicine for its antioxidant and anticancer properties. Its extract, considered a valuable food byproduct, holds significant potential for development and utilization. In this study, we conducted a search and analysis of the active ingredients of LS, revealing several anti-photoaging components such as quercetin, β-sitosterol, procyanidin A1, stigmasterol, and ent-epicatechin. These findings suggest promising effects in delaying photoaging.

The anti-photoaging active ingredients predicted in this study are concentrated in naturally occurring polyphenols and phytosterols. Research has demonstrated the effectiveness of naturally occurring polyphenols like grape seed proanthocyanidins were effective against inflammation induced by UV radiation, oxidative stress, DNA damage, and suppression of immune response[31-33]. Quercetin belongs to the flavonoid family of polyphenols. Quercetin treatment inhibited UV-induced expression of matrix metalloproteinase-1 (MMP-1) and cyclooxygenase-2 (COX-2) and prevented UV-mediated degradation of collagen in human skin tissue[34]. Meanwhile, quercetin can directly target PKCδ and JAK2 in the skin to reduce UV-induced skin aging and inflammation. Besides, phytosterols such as aloe sterol, saltwort sterol, and soy sterol are mainly shown to reduce excessive elevation of pro-inflammatory cytokines (IL-1β and TNF-α) and matrix metalloproteinases (MMP-2,

MMP-9, MMP-12, and MMP-13) in photodamaged skin exposed to light[35-36]. MMP release from epidermal keratinocytes and dermal fibroblasts leads to changes in skin composition and degradation of the ECM compounds including collagen and elastin fibers in the skin dermis[37]. UV radiation upregulates the expression of various MMPs, MMPs also lead to the loss of collagen synthesis activity loss of collagen synthesis activity, ultimately inducing photoaging. Ultraviolet A (UVA) radiation is the primary inducer of skin photoaging pathogenesis. Repeated ultraviolet radiation overactivates the complement system, causing damage to the dermal-epidermal junction and deposition on it, resulting in chronic inflammation and long-term damage to the dermis; macrophages are overburdened by oxidized lipids, and overloaded macrophages release pro-inflammatory cytokines and ROS, triggering oxidative stress and inducing extracellular matrix damage in the dermis[38]. Long-term chronic inflammation is one of the triggers for cancer development, and long-term photodamage not only leads to the development of skin problems, but may also induce skin cancer.

In the PPI network and KEGG pathway cnet diagram, IL6, AKT1, CASP3, and TP53 were identified as core targets. The core protein AKT plays a pivotal role in apoptosis, with the AKT signaling pathway being crucial in the regulation of aging. During cellular aging, activation of the phosphatidylinositol-3-kinase (PI3K) signaling pathway enhances the accumulation of reactive oxygen species (ROS), which contributes to the aging of human skin fibroblasts. Phosphorylated AKT (P-Akt) inhibits the expression and activation of various pro-apoptotic proteins, thereby exerting anti-apoptotic effects. Caspase-3, a cysteine-aspartate protease, is a key executor of apoptosis and is widely recognized as a biomarker of this process. The TP53 gene encodes a transcription factor that regulates cell cycle initiation. The P53 protein, translated from the TP53 gene, is a crucial regulator of cell growth, proliferation, and damage repair. IL-6 is a multifunctional cytokine involved in immunity, tissue regeneration, and metabolism. Notably, as a pro-inflammatory cytokine, IL-6 plays a significant role in chronic inflammatory responses. Exogenous inflammatory signals can promote cellular senescence, highlighting the complex interplay between inflammation and aging[39-41]. The identification of these core targets aligns with the pathogenesis of skin photoaging, which involves oxidative stress, inflammation, and impaired cellular repair mechanisms. The PI3K/AKT pathway's role in ROS accumulation underscores its contribution to oxidative damage in skin cells. Meanwhile, the anti-apoptotic function of P-Akt suggests a protective mechanism against cell death, potentially counteracting the detrimental effects of UV-induced damage. Caspase-3's involvement in apoptosis further illustrates the importance of regulated cell death in maintaining skin homeostasis and preventing premature aging. TP53's regulation of cell cycle and damage repair mechanisms is critical in responding to UV-induced DNA damage, thereby maintaining genomic integrity. IL-6's dual role in immunity and chronic inflammation reflects its contribution to the inflammatory milieu associated with photoaging. Elevated levels of IL-6 in response to UV exposure can exacerbate inflammatory responses, accelerating the aging process. In summary, the interplay of IL6, AKT1, CASP3, and TP53 within the context of skin photoaging highlights the intricate balance between oxidative stress, inflammation, and cellular repair mechanisms. Targeting these pathways could provide therapeutic strategies to mitigate photoaging and promote skin health.

The results of BP enrichment analysis showed that the LS in the treatment of photoaging is mainly associated with response to reactive oxygen species, response to oxidative stress, epithelial cell proliferation and response to UV. The light absorbed into the skin transmits its energy to various plastids, such as amino acids, nucleic acids, and melanin. Then, these plastids produce free radicals, causing photolysis and reacting with free oxygen molecules in the living body to form ROS [42]. The pathway of gene expression induced by ROS leads to increased collagen degradation and accumulation of elastic proteins, which is an important pathway for oxidative stress and inflammatory response [43].

As shown in the KEGG analysis result, the targets of LS-photoaaging were enriched in pathways closely relevant to photoaging, such as immune-inflammatory pathways and apoptosis. Overloaded UV stress cells release pro-inflammatory cytokines and ROS, triggering oxidative stress, cause apoptosis and inducing extracellular matrix damage in the dermis. After identifying core targets and active compounds, molecular docking was used to assess core targets interactions. The docking results showed that the small molecule ligands formed stable hydrogen bonds with the receptors. This further confirms that LS may affect the function through the interaction with photoaging-related genes, thereby producing drug activity.

5. Conclusion

In this study, the molecular mechanisms underlying the protective effects of Litchi Seed (LS) on skin photoaging were systematically analyzed using network pharmacology in combination with GEO database mining. This approach provided comprehensive evidence supporting the efficacy of LS in combating skin photoaging. The results demonstrated that LS could mitigate photoaging by reducing oxidative stress and lowering levels of TNF and IL-6. The corresponding mechanisms likely involve the activation of the ROS/MAPK/AP-1 and PI3K-Akt signaling pathways. Furthermore, it was found that quercetin, β-sitosterol, procyanidin A1, stigmasterol, and ent-epicatechin form stable docking models with AKT1, IL6, TP53, and CASP3, respectively. This finding further confirms that LS can interact with photoaging-related target proteins, influencing their function and exerting protective effects against photoaging. The study elucidated the synergistic mechanisms of the multi-component, multi-target, and multi-pathway actions of LS in delaying photoaging. However, this investigation serves as a preliminary screening and prediction of LS's role in delaying photoaging. Subsequent biological experiments are necessary to further validate the identified targets and pathways to confirm our conclusions.

List of Abbreviations

Litchi seed = LS
Ultraviolet Radiation = UVR
Traditional Chinese Medicine Database and Analysis Platform = TCMSP
Universal Protein Resource = UniProt
Gene Expression Omnibus = GEO
Gene Ontology = GO
Kyoto Encyclopedia of Genes and Genomes = KEGG
Molecular Weight = MW
Drug-likeness = DL
Differentially expressed genes = DEGs
Online Mendelian Inheritance in Man = OMIM
Degree Centrality = DC
Betweenness Centrality = BC
Closeness Centrality = CC

Ethics Approval and Consent to Participate

Not applicable.

Human and Animal Rights

No animals/humans were used for studies that are the basis of this research.

References

[1] Furukawa, J. Y.; Martinez, R. M.; Morocho-Jacome, A. L.; et al., Skin impacts from exposure to ultraviolet, visible, infrared, and artificial lights - a review. *Journal of Cosmetic and Laser Therapy* **2021,** *23* (1-2), 1-7.http://doi.org/10.1080/14764172.2021.1950767.

[2] Pedic, L.; Pondeljak, N.; Situm, M., Recent information on photoaging mechanisms and the preventive role of topical sunscreen products. *Acta Dermatovenerologica Alpina Pannonica Et Adriatica* **2020,** *29* (4), 201-207.http://doi.org/10.15570/actaapa.2020.40.

[3] Salminen, A.; Kaarniranta, K.; Kauppinen, A., Photoaging: UV radiation-induced inflammation and immunosuppression accelerate the aging process in the skin. *Inflammation Research* **2022,** *71* (7-8), 817-831.http://doi.org/10.1007/s00011-022-01598-8.

[4] Sachs, D. L.; Varani, J.; Chubb, H.; et al., Atrophic and hypertrophic photoaging: Clinical, histologic, and molecular features of 2 distinct phenotypes of photoaged skin. *Journal of the American Academy of Dermatology* **2019,** *81* (2), 480-488.http://doi.org/10.1016/j.jaad.2019.03.081.

[5] Petruk, G.; Del Giudice, R.; Rigano, M. M.; Monti, D. M., Antioxidants from Plants Protect against Skin Photoaging. *Oxidative Medicine and Cellular Longevity* **2018,** *2018*.http://doi.org/10.1155/2018/1454936.

[6] Dyjakon, A.; Sobol, L.; Noszczyk, T.; Mitrega, J., The Impact of Torrefaction Temperature on the Physical-Chemical Properties of Residual Exotic Fruit (Avocado, Mango, Lychee) Seeds. *Energies* **2022,** *15* (2).http://doi.org/10.3390/en15020612.

[7] Bosch, R.; Philips, N.; Suarez-Perez, J. A.; Juarranz, A.; et al., Mechanisms of Photoaging and Cutaneous Photocarcinogenesis, and Photoprotective Strategies with Phytochemicals. *Antioxidants (Basel, Switzerland)* **2015,** *4* (2), 248-68.http://doi.org/10.3390/antiox4020248.

[8] Chen, Y.; Li, H.; Zhang, S.; et al., Anti-myocardial Ischemia Effect and Components of Litchi Pericarp Extracts. *Phytotherapy Research* **2017,** *31* (9), 1384-1391.http://doi.org/10.1002/ptr.5865.

[9] Yarovaya, L.; Waranuch, N.; Wisuitiprot, W.; Khunkitti, W., Clinical study of Asian skin changes after application of a sunscreen formulation containing grape seed extract. *Journal of Cosmetic Dermatology* **2022,** *21* (10), 4523-4535.http://doi.org/10.1111/jocd.14982.

[10] Xie, Y.; Zhu, G.; Yi, J.; et al., A new product of multi-plant extracts improved skin photoaging: An oral intake in vivo study. *Journal of Cosmetic Dermatology* **2022,** *21* (8), 3406-3415.http://doi.org/10.1111/jocd.14620.

[11] Liu, S.; You, L.; Zhao, Y.; Chang, X., Hawthorn Polyphenol Extract Inhibits UVB-Induced Skin Photoaging by Regulating MMP Expression and Type I Procollagen Production in Mice. *Journal of Agricultural and Food Chemistry* **2018,** *66* (32), 8537-8546.http://doi.org/10.1021/acs.jafc.8b02785.

[12] Bernatova, I., Biological activities of (−)-epicatechin and (−)-epicatechin-containing foods: Focus on cardiovascular and neuropsychological health. *Biotechnology Advances* **2018,** *36* (3), 666-681.http://doi.org/https://doi.org/10.1016/j.biotechadv.2018.01.009.

[13] Wang, X.; Wang, Z.-Y.; Zheng, J.-H.; Li, S., TCM network pharmacology: A new trend towards combining computational, experimental and clinical approaches. *Chinese Journal of Natural Medicines* **2021,** *19* (1), 1-11.http://doi.org/10.1016/s1875-5364(21)60001-8.

[14] Zheng, L.; Meng, J.; Jiang, K.; et al., Improving protein-ligand docking and screening accuracies by incorporating a scoring function correction term. *Briefings in Bioinformatics* **2022,** *23* (3).http://doi.org/10.1093/bib/bbac051.

[15] Shikov, A. N.; Flisyuk, E. V.; Obluchinskaya, E. D.; Pozharitskaya, O. N., Pharmacokinetics of Marine-Derived Drugs. *Marine Drugs* **2020,** *18* (11).http://doi.org/10.3390/md18110557.

[16] Zong, K.; Xu, K.; Zhang, X.; et al., Explorating the mechanism of Huangqin Tang against skin lipid accumulation through network pharmacology and experimental validation. *Journal of Ethnopharmacology* **2023,** *313*.http://doi.org/10.1016/j.jep.2023.116581.

[17] Hua, L. I. U.; WenLi, M. A.; WenLing, Z., GEO (Gene Expression Omnibus) : High-throughput Gene Expression Database. *Chinese Journal of Biochemistry and Molecular Biology* **2007,** *23* (3), 236-244.

[18] Warrick, E.; Duval, C.; Nouveau, S.; et al., Actinic lentigines from Japanese and European volunteers share similar impaired biological functions. *Journal of Dermatological Science* **2022,** *107* (1), 8-16.http://doi.org/10.1016/j.jdermsci.2022.07.001.

[19] Sean, D.; Meltzer, P. S., GEOquery: a bridge between the gene expression omnibus (GEO) and BioConductor. *Bioinformatics* **2007,** *23* (14), 1846-1847.http://doi.org/10.1093/bioinformatics/btm254.

[20] Ritchie, M. E.; Phipson, B.; Wu, D.; et al., limma powers differential expression analyses for RNA-sequencing and microarray studies. *Nucleic Acids Research* **2015,** *43* (7).http://doi.org/10.1093/nar/gkv007.

[21] Gu, Z.; Eils, R.; Schlesner, M., Complex heatmaps reveal patterns and correlations in multidimensional genomic data. *Bioinformatics* **2016,** *32* (18), 2847-2849.http://doi.org/10.1093/bioinformatics/btw313.

[22] Tang, Y.; Li, M.; Wang, J.; Pan, Y.; Wu, F.-X., CytoNCA: A cytoscape plugin for centrality analysis and evaluation of protein interaction networks. *Biosystems* **2015,** *127*, 67-72.http://doi.org/10.1016/j.biosystems.2014.11.005.

[23] Wang, W.; Li, M.; Si, H.; Jiang, Z., Network Pharmacology and Integrated Molecular Docking Study on the Mechanism of the Therapeutic Effect of Fangfeng Decoction in Osteoarthritis. *Current Pharmaceutical Design* **2023,** *29* (5), 379-392.http://doi.org/10.2174/1381612829666230216095659.

[24] Shi, L.; Si, H., 3D-QSAR Studies on High-affinity Phosphodiestera. *Current medicinal chemistry* **2024**.http://doi.org/10.2174/0109298673275082231220074933.

[25] Seeliger, D.; de Groot, B. L., Ligand docking and binding site analysis with PyMOL and Autodock/Vina. *Journal of Computer-Aided Molecular Design* **2010,** *24* (5), 417-422.http://doi.org/10.1007/s10822-010-9352-6.

[26] Tao, W.; Xu, X.; Wang, X.; et al., Network pharmacology-based prediction of the active ingredients and potential targets of Chinese herbal Radix Curcumae formula for application to cardiovascular disease. *Journal of Ethnopharmacology* **2013,** *145* (1), 1-10.http://doi.org/10.1016/ j.jep.2012.09.051.

[27] Chin, C.-H.; Chen, S.-H.; Wu, H.-H.; et al., cytoHubba: identifying hub objects and sub-networks from complex interactome. *Bmc Systems Biology* **2014,** *8*.http://doi.org/10.1186/ 1752-0509-8-s4-s11.

[28] Wei, G.; Shu-sen, X. I. E., Progress on Skin Photoaging Evaluation and Treatment Based on Optical Technology. *Acta Laser Biology Sinica* **2009,** *18* (5), 690-694

[29] Chen, X.; Yang, C.; Jiang, G., Research progress on skin photoaging and oxidative stress. *Postepy Dermatologii I Alergologii* **2021,** *38* (6), 931-936.http://doi.org/10.5114/ada.2021.112275.

[30] Yao, W.; Chen, X.; Li, X.; et al., Current trends in the anti-photoaging activities and mechanisms of dietary non-starch polysaccharides from natural resources. *Critical Reviews in Food Science and Nutrition* **2022,** *62* (32), 9021-9035.http://doi.org/10.1080/10408398.2021.1939263.

[31] Pirniyazov, A. Z.; Abdulladzhanova, N. G.; Mavlyanov, S. M.; Kamaev, F. G.; Dalimov, D. N., Polyphenols from Vitis vinifera seeds. *Chemistry of Natural Compounds* **2003,** *39* (4), 349-354.http://doi.org/10.1023/b:Conc.0000003414.46129.15.

[32] Unusan, N., Proanthocyanidins in grape seeds: An updated review of their health benefits and potential uses in the food industry. *Journal of Functional Foods* **2020,** *67*.http://doi.org/10.1016/j.jff.2020.103861.

[33] Mahdipour, R.; Ebrahimzadeh-Bideskan, A.; Hosseini, M.; et al., The benefits of grape seed extract in neurological disorders and brain aging. *Nutritional Neuroscience* **2023,** *26* (5), 369-383.http://doi.org/10.1080/1028415x.2022.2051954.

[34] Vicentini, F. T. M. C.; He, T.; Shao, Y.; et al., Quercetin inhibits UV irradiation-induced inflammatory cytokine production in primary human keratinocytes by suppressing NF-κB pathway. *Journal of Dermatological Science* **2011,** *61* (3), 162-168.http://doi.org/10.1016/j.jdermsci.2011.01.002.

[35] Sin, B. Y.; Kim, H. P., Inhibition of collagenase by naturally-occurring flavonoids. *Archives of Pharmacal Research* **2005,** *28* (10), 1152-1155.http://doi.org/10.1007/bf02972978.

[36] Shin, E. J.; Lee, J. S.; Hong, S.; Lim, T.-G.; Byun, S., Quercetin Directly Targets JAK2 and PKCδ and Prevents UV-Induced Photoaging in Human Skin. *International Journal of Molecular Sciences* **2019,** *20* (21).http://doi.org/10.3390/ijms20215262.

[37] Kohl, E.; Steinbauer, J.; Landthaler, M.; Szeimies, R. M., Skin ageing. *Journal of the European Academy of Dermatology and Venereology* **2011,** *25* (8), 873-884. http://doi.org/10.1111/j.1468-3083.2010.03963.x.

[38] Zhang, S.; Duan, E., Fighting against Skin Aging: The Way from Bench to Bedside. *Cell Transplantation* **2018**.http://doi.org/10.1177/0963689717725755.

[39] Jenny, N. S., Inflammation in Aging: Cause, Effect, or Both? *Discovery Medicine* **2012,** *13* (73), 451-460

[40] Zhao, Y.; Simon, M.; Seluanov, A.; Gorbunova, V., DNA damage and repair in age-related inflammation. *Nature Reviews Immunology* **2023,** *23* (2), 75-89.http://doi.org/10.1038/s41577- 022-00751-y.

[41] Mocchegiani, E., Cellular Senescence and Inflammation: Advances and Therapeutic Targets in Aging and Major Age-Related Diseases. *Current Pharmaceutical Design* **2013,** *19* (9), 1673-1674

[42] Choi, S.-I.; Lee, J.-H.; Kim, J.-M.; et al., Ulmus macrocarpa Hance Extracts Attenuated H2O2 and UVB-Induced Skin Photo-Aging by Activating Antioxidant Enzymes and Inhibiting MAPK Pathways. *International Journal of Molecular Sciences* **2017**.http://doi.org/10.3390/ijms18061200.

[43] Li, C.; Fu, Y.; Dai, H.; Wang, Q.; et al., Recent progress in preventive effect of collagen peptides on photoaging skin and action mechanism. *Food Science and Human Wellness* **2022,** *11* (2), 218-229.http://doi.org/10.1016/j.fshw.2021.11.0032213-4530.